Online energy reconstruction for calorimeters under high pile-up conditions using deconvolutional techniques

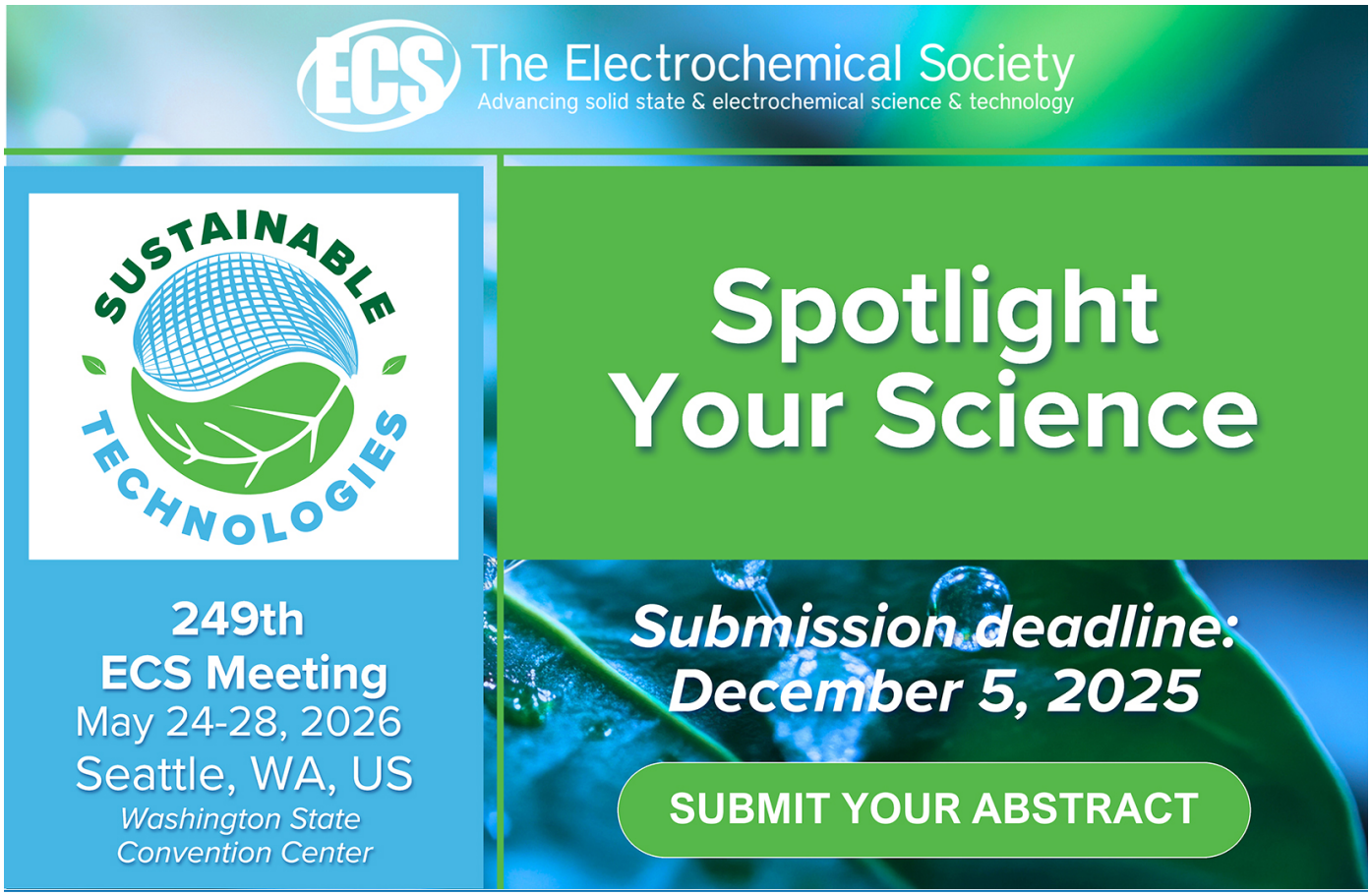

Published by IOP Publishing for Sissa Medialab

Received: *August 20, 2019*
Revised: *October 25, 2019*
Accepted: *November 22, 2019*
Published: *December 23, 2019*

Online energy reconstruction for calorimeters under high pile-up conditions using deconvolutional techniques

J.P.B.S. Duarte,[a,1] **L.M. de Andrade Filho,**[a] **E.F. de Simas Filho,**[b] **P.C.M.A. Farias**[b] **and J.M. de Seixas**[c]

[a] *Signal Processing Lab, PPEE, Federal University of Juiz de Fora, Juiz de Fora, Brazil*
[b] *Digital Systems Lab, PPGEE, Federal University of Bahia, Salvador, Brazil*
[c] *Signal Processing Lab, COPPE/Poli, Federal University of Rio de Janeiro, Rio de Janeiro, Brazil*

E-mail: joao.duarte@engenharia.ufjf.br

Abstract: High-energy calorimeters operating at high data acquisition rate may suffer from signal superposition (pile-up) in their electronic readout. This problem occurs whenever the time interval among two subsequent incoming physics signatures is shorter than the front-end electronics time latency. Signal pile-up may cause severe problems on the online energy estimation and some palliative solutions, treating the pile-up signals as an additional noise source, have been proposed in order to preserve the well established Optimal Filter theory as the signal estimation baseline design. In order to produce actual online compensation for pile-up effect, the method proposed in this paper approximates the front-end electronics as a linear transmission channel whose transfer function can be linearly equalized (unconvolved). For experiments where the acquisition rate is synchronized with the collision clock, the equalizer output provides a straightforward energy estimation per bunch-crossing (BC). Optimal approximations for the equalizer design are proposed using both FIR (Finite Impulse Response) filters and an iterative method. The latter offers better reconstruction performance (smaller errors), but has higher computational cost and requires extra data-flow circuitry when online implementation is envisaged. Toy simulation data that consider typical calorimeter front-end responses are used to evaluate the performance of the proposed methods.

Keywords: Data processing methods; Online farms and online filtering; Digital signal processing (DSP)

[1] Corresponding author.

https://doi.org/10.1088/1748-0221/14/12/P12017

2019 JINST 14 P12017

Contents

2019 JINST 14 P12017

1 Introduction

High-energy physics (HEP) experiments search for the fundamental components of matter and the understanding of their forms of interaction. In order to achieve these goals, HEP experiments rely very much on their instrumentation and signal processing systems to provide accurate and relevant information for the characterization of known processes and also for the search for new physics. Modern HEP experiments are often huge facilities designed and operated by international scientific collaborations [1–4].

A great number of important discoveries in HEP came from particle collider experiments [5], which are designed to accelerate and collide bunches of particles. The information generated from these collisions is sampled by the particle detectors. A typical particle experiment design comprises different sub-detectors, and among them calorimeters play a major role, as they measure both energy and position of the incoming particles through fine-grained segmentation [6].

As a huge amount of information is generated in particle collider experiments and the interesting events are often very rare, an online event selection (trigger) system is required to select relevant physics information and reject, as much as possible, the enormous background noise (non-interesting physics) [7–9]. Typically, such trigger systems are designed to operate in sequential selection stages, in which non-relevant events are gradually discarded [10]. In order to deal with high event rates, the first trigger level is usually implemented in dedicated hardware [11]. The following levels are typically designed to operate in software using massive parallel computational systems [7, 12].

Calorimeters usually participate in all trigger levels, as they provide a fast response and their energy deposition profile is used for particle discrimination. Typically, calorimeters need a conditioning circuit (shaper) to improve the energy estimation accuracy [6]. The shaper unit is responsible for producing a fixed-shape readout signal response after a particle interation in a given calorimeter sensor. Thus, the calorimeter readout assumes a fixed pulse shape, for which the signal amplitude is proportional to the deposited energy in the respective sensor (or calorimeter cell) [13].

Concerning the first-level trigger, usually two tasks are performed by the calorimeter acquisition system [14]: i) the detection of a signal (time-stamp for an incoming pulse), so that one can infer to which collision the particles belong to, and ii) the amplitude estimation of the detected signal, in order to compute the energy deposited in the calorimeter cell. Those tasks should be performed in a fast and uninterrupted engine, which is referred to here as a free-running procedure. In the case of acceptance by the first-level trigger, Analog-to-Digital Converter (ADC) samples around the detected peak are collected and passed through higher trigger levels, where more sophisticated signal reconstruction procedures can be performed.

Free-running detection and estimation procedures are usually implemented using FIR (Finite Impulse Response) filters [15] followed by a peak detector circuitry [16]. FIR filters are designed in a manner that, when the entire incoming pulse fits within the FIR filter taps, the output of the filter provides an estimation of the amplitude of the pulse based on a given optimization criterion. Several optimization techniques such as Matched Filters (MF), Autocorrelation Filters (AF), Best Linear Unbiased Estimation (BLUE), Variance Minimization of estimators (Optimal Filters — OF), Maximum Likelihood Estimation (MLE), have shown to converge to basically the same filter design, when a linear structure (FIR filters) is the constraint [17–20]. In the filter output, a digital peak detector must be implemented in order to detect the pulse time-stamp, vanishing the estimation for adjacent BCs.

1.1 High-luminosity experiments

Modern particle colliders may require increasing levels of both energy and luminosity [5], in order to boost the probability of producing relevant (new physics) information. In this scenario, the experiments are required to cope with a very high detector occupancy, which may generate a superposition of signals (also known as pile-up) [21, 22] in calorimeters, as the time interval among two consecutive interactions in the same detector region may become shorter than the system readout time-response [23]. Such signal overlapping degrades the original pulse shape, deteriorating the performance of standard energy and time-stamp estimation methods used in signal reconstruction. In the past, where pile-up was not so frequent, piled-up information was simply discarded without any relevant impact for the experiment.

2019 JINST 14 P12017

However, in high-luminosity colliders, like the Large Hadron Collider (LHC) [24] and the Future Circular Collider (FCC) [4], the superposition of signals in calorimeters has become a baseline and data must be reconstructed even under such harsh pile-up conditions. This represents a new challenge in calorimetry. Thus, the general-purpose LHC experiments (ATLAS [25] and CMS [26]) are presently looking forward to implement efficient reconstruction methods capable to address this issue. However, the present baseline designs still adapt the well established OF [10, 27] techniques to such pile-up conditions.

In ATLAS, for instance, second-order statistics from pile-up signals are extracted and interpreted as a highly correlated noise in the filter design [28, 29]. The use of pile-up information as additional noise source has shown to mitigate the pile-up effect on the energy estimation, for both online and offline reconstructions. However, the pile-up noise has higher-order statistics that cannot be accessed from linear optimization techniques, since they use only the second-moment information (imposed by the linear constraint). Besides, the effect of combining this procedure with a peak detector degrades the final performance, since this circuitry supposes the presence of only empty bunches around the peak value. In CMS, the same OF principle, based on variance minimization, is used, but now a multi-amplitude filter has been proposed in order to estimate the amplitude of three consecutive signals: the central one and the two side neighbor signals [30]. Despite simplicity, such OF approach ignores the presence of signal tails from other BCs and should be used only in calorimeters with very sharp signals. The method proposed in ATLAS is more general and will be used here as reference for comparison with the proposed method.

1.2 Signal deconvolution

Aiming at reducing further the pile-up effect, a method based on signal deconvolution has already been proposed for offline energy estimation [31], in which an approximate inverse model (deconvolution) of the calorimeter readout channel was used. Different from OF based methods, pile-up is not treated as noise in the deconvolution process. Instead, the whole signal information is used in a Source Separation (SS) routine. Thus, the performance is improved with respect to variance minimization techniques (OF), which only use second-order statistics of the pile-up samples in the filter design.

Deconvolution has been extensively employed in signal processing for digital communication [32]. The transmitted signal is modified by the communication channel and the signal in the receiver end is modeled as the convolution between the transmitted (target) information and the channel impulse response. Deconvolution methods are employed in the receiver in order to recover the target information. Actually, in [31], the whole calorimeter signal generation chain is treated as a communication channel whose target signal (energy per BC) can be reconstructed using deconvolution, opening a new field of signal processing for nuclear electronics.

Sparse Representation (SR) [33] methods have been proposed for offline [34] as well, where deconvolution is obtained performing a linear transformation that maximizes the number of empty bunches, reconstructing the impulsive characteristic of the target signal. SR is able to perform the deconvolution process together with noise mitigation, becoming one of the most efficient methods for signal equalization. Although efficient for signal reconstruction under pile-up, these are typical offline methods, which require high computational resources and are not suitable for online and parallel operation.

2019 JINST 14 P12017

This work proposes signal processing techniques to perform free-running deconvolution, in the sense that the system output delivers reconstructed energy information for every collision during a given run, as long as the system clock is synchronous with the collider BC. The proposed methods are intended to be used in online environments, like trigger systems, where hardware resource minimization is an issue and fast processing is a severe constraint. Two alternative deconvolution methods are proposed. One is based on FIR filters, envisaging low cost implementation. For FIR filters, the free-running data flow is straightforward, since this kind of filter structure generates one new output to each clock tick. The second method uses iterative Gradient Descent (GD) algorithms [32], which produce an energy estimation more resilient for different operational conditions, but require more computational resources. Although the latter works similarly to the offline techniques (all BCs within a window are estimated simultaneously, requiring several clock periods to perform the iterations and to deliver all the reconstructed energy information in parallel), the one proposed here requires only addition and multiplication operations. This allows free-running implementation in high-speed modern FPGA's (Field Programmable Gate Arrays), when extra data-flow circuitry is used for serialization and de-serialization procedures [35].

Two FIR filter design methods were applied aiming at calorimeter channel equalization. In the first one, to obtain the filter coefficients, only the calorimeter reference readout channel pulse shape is necessary. However, if on top of pile-up additional noise sources are present, they will not be considered. Thus, a second FIR filter design method is proposed to minimize the mean square error (MSE) between the signal reconstruction and the signal truth, which may be accessed from simulated data. The former uses the reference calorimeter pulse-shape information only and the design is independent of other environment parameters. On the other hand, the latter, which is known as the Least Square (LS) filter [36], tends to present better performance, but requires an accurate simulation of the target environment.

Differently from the FIR filters, the proposed GD method produces simultaneous energy estimation for several collisions within a given acquisition window. Since negative amplitude estimation has no meaning in calorimetry, negative values can be removed at each iteration, implementing a kind of non-linear reconstruction that intrinsically accesses the higher-order statistics of the pile-up noise, providing better performance. Besides, the vanishing of negative BC values connects the method with modern SR techniques, which has shown to be an efficient deconvolution procedure for impulsive target signals [34].

This paper is organized as follows. The online energy estimation is revised in the next section, for reference. Section 2.2 details the calorimeter channel response model, which is used for deconvolution. The FIR filter deconvolution approach for free-running energy estimation under pile-up is presented in section 3. The inverse channel modeling and the LS filter are both detailed there. Section 4 concerns the GD methods. Results from simulated data are presented in section 5 and conclusions are derived in section 6.

2 Online energy estimation

This section addresses both the standard approach used for energy estimation, which considers the pile-up as an additive noise, and the alternative model, based on channel response, which is the base for the online deconvolution reconstruction methods proposed in this paper.

2019 JINST 14 P12017

2.1 Standard estimation method

The standard estimation procedure is based on some statistical optimization criteria, where only second order statistics is employed to ensure a linear implementation. In this context, OF, MF for Gaussian Noise and AF, are the commonly employed approaches. In any case, the performance are the same achieved by a more general linear estimation theory, the BLUE method, that will be described here in more details.

A procedure commonly adopted in calorimeters is to perform online energy estimation in two processing steps [37]: apply a linear signal amplitude estimation using the most recent consecutive digitized samples of the front-end electronics from a given calorimeter cell, followed by a peak detector, which detects the time-stamp for which the amplitude estimation is valid. Figure 1a sketches graphically the energy sampled by a calorimeter sensor (Target) in a given collision index and what is really seen at the sensor front-end output after the ADC (Measured). The abscissa represents both the BC time-stamp and the discrete time basis k for the ADC output, since those values are synchronized. In this plot, the LHC collision rate of 40 MHz is used. The calorimeter readout signal represented here is unipolar, since it is the most common case [17, 38, 39]. Typically, the calorimeter signal spreads over several consecutive BCs. For figure 1, an unipolar pulse with a 150 ns spread is assumed.

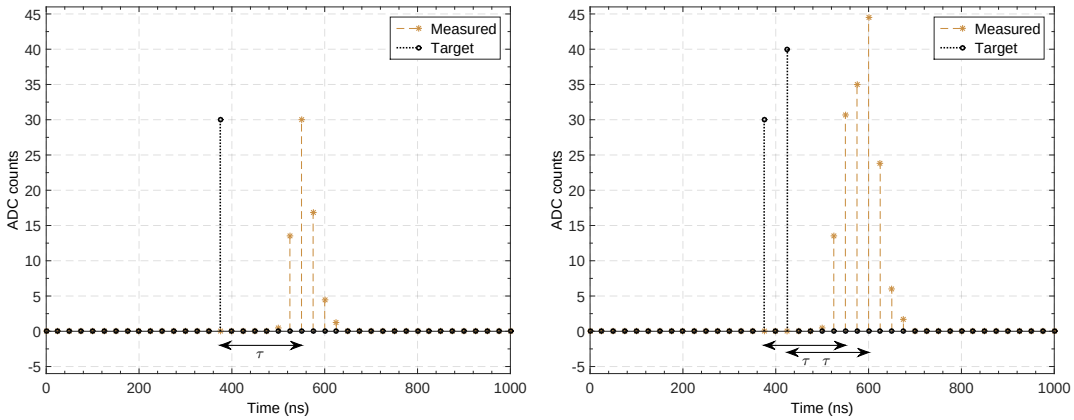

Figure 1. ADC samples are synchronized with the collision clock, but there is a system delay τ: (a) a single signal, and the maximum measured value corresponds to the target energy value. (b) signal overlapping in high-luminosity conditions.

The calorimeter sensor has a response delay (τ), which is calibrated to match the signal peak and represents the delay between the collision time-stamp and the respective signal in the front-end output. Therefore, detecting the peak position in the measured sequence and estimating its amplitude is the standard procedure for energy reconstruction from the sensor's digitized output. For online reconstruction proposals, Shifter Registers are used to store the set of the M most recent consecutive digitized samples, as shown in figure 2. In this figure, $y[k]$ represents the most recent sample delivered by the free-running ADC, connected to a calorimeter sensor front-end. For standard reconstruction procedures, the value of M depends on the number of samples necessary to represent the entire pulse. For bipolar pulses with long negative tails, only the positive lobule

2019 JINST 14 P12017

samples are considered [40], since most of the information is contained in this part of the pulse (samples above the noise). This figure also shows how the M coefficients w_j of the filter are structured in order to provide the linear amplitude estimation at each clock. As expected, this is a suitable structure for a FIR filter implementation. The ADC clock is synchronized with the collider clock in such a way that a BC energy estimation is assigned to each FIR filter output sample. However, since the design of the filter coefficients is based on amplitude estimation of a shape-deterministic signal, the FIR filter output is valid only when the entire pulse is within the filter taps. Thus, a peak detector circuitry is necessary, delivering the FIR filter output only when a signal peak is found and discarding the other output values in the acquired window.

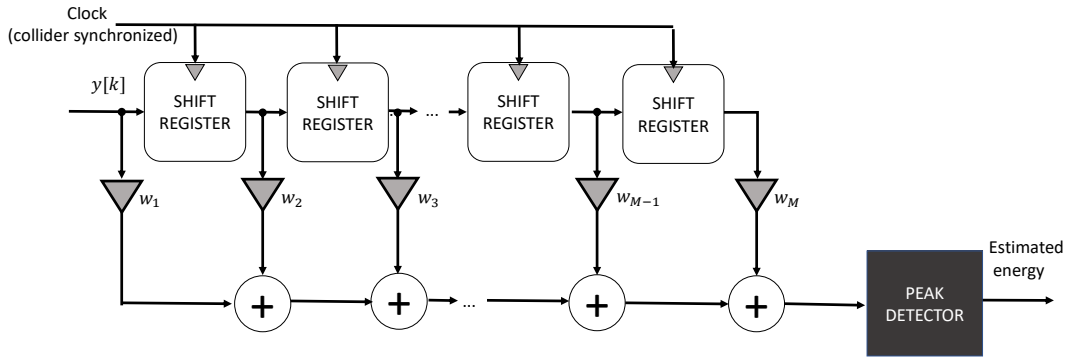

Figure 2. Standard online energy reconstruction scheme.

The filter coefficients are obtained through a proper optimization criterion. The BLUE is the most suitable method in this context [36]. Other more general amplitude estimation procedures can also be found in literature [41–43]. However, they have to apply a linearity constraint, which results in the same set of BLUE coefficients [20].

Considering the digitized calorimeter reference pulse shape (fixed) as a vector $\mathbf{h}$ of length M and taking M most recent produced samples as a vector $\mathbf{y}$ (the values buffered on the FIR filter taps, in this case), a linear model for $\mathbf{y}$, when the entire pulse is within the filter taps, is given by

$$\mathbf{y} = A\mathbf{h} + \boldsymbol{\epsilon}, \tag{2.1}$$

where $\boldsymbol{\epsilon}$ is the embedded noise, which currently, in LHC experiments, has been used to represent the pile-up information (Out-Of-Time signals — OOT) together with the additive electronic readout noise. The target signal amplitude is denoted by A. According to the BLUE theory, for zero-mean noise, the unbiased estimated amplitude $\hat{A}$ is given by:

$$\hat{A} = \frac{\mathbf{h}^T \mathbf{C}_\epsilon^{-1} \mathbf{y}}{\mathbf{h}^T \mathbf{C}_\epsilon^{-1} \mathbf{h}} = \boldsymbol{w}^T \mathbf{y}, \tag{2.2}$$

where T is the transpose operator and $\mathbf{C}_\epsilon$ is the $M \times M$ noise covariance matrix. The term $\boldsymbol{w}$ is the vector of size M that characterizes the filter weights to be used.

For white noise, $\mathbf{C}_\epsilon$ is proportional to the Identity matrix and the BLUE coefficients have the shape of the calorimeter reference pulse $\mathbf{h}$. When pile-up arises, those signals are treated as a highly correlated noise on the amplitude estimation of the central signal and $\mathbf{C}_\epsilon$ absorbs their second-order statistics, which is obtained either from real data or simulation [44].

2019 JINST 14 P12017

2.2 Channel response model

In this model, OOT signals are not considered as noise. The noise vector samples, named here $e[k]$, contain electronic noise only. Besides, for the FIR filter structure that is being proposed here, the filter order does not necessarily match the reference signal length (M), as it will be shown below.

Figure 1b shows what happens when the calorimeter sensor is excited by two consecutive collisions. The sensor shaped signals overlap to each other and the target energy may not be reconstructed properly using standard methods (signal amplitude estimation). The model in [31] aims at compensating for such pile-up effect. This is achieved by a non-causal linear time-invariant (LTI) discrete-time system [15], which represents a calorimeter channel response, as shown in figure 3. In this figure, an arbitrary unipolar shaping calorimeter readout pulse is considered, but the proposed model works for any calorimeter with deterministic pulse shape (including bipolar signals). In order to link the energy reconstruction problem to this digital signal processing perspective, the target signal (energy per BC) is interpreted here as a discrete sequence $a[k]$. When $a[k]$ is the Dirac Delta impulsive function $\delta[k]$, the LTI output is the so called impulsive response $h[k]$. In this model, the constant delay τ is previously removed and the model becomes non-causal, with the peak position of $h[k]$ at the same index of the impulse. Therefore, the deconvolution process reconstructs the target energy at the correct time-stamp. In [31], $h[k]$ is modeled as the calorimeter reference pulse shape with the peak centered at $k = 0$ and $a[k]$ is taken as a linear combination of delayed versions of the $\delta[k]$, whose amplitudes correspond to the energy at each BC. Thus, the output $y[k]$ is obtained from convolution:

$$y[k] = \sum_{l=-L_b}^{L_a} (h[l]a[k-l]) + e[k], \tag{2.3}$$

where L_b and L_a are the number of samples before and after the peak for the reference signal, respectively. Here, $e[k]$ is the electronic readout noise only.

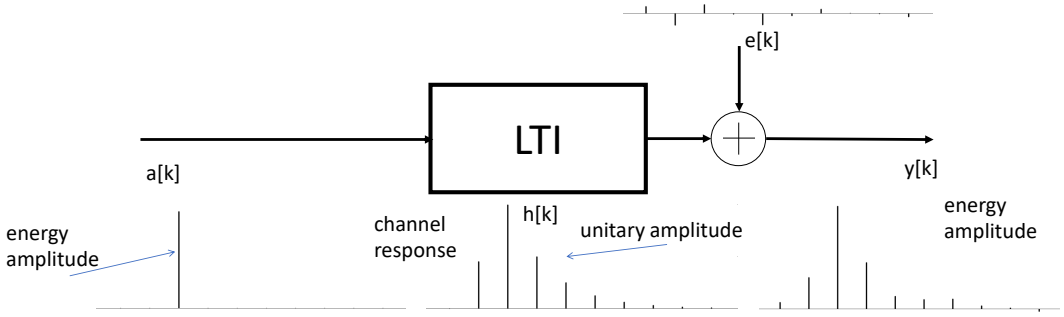

Figure 3. A LTI system model connecting the target information (energy per BC — $a[k]$) to an arbitrary calorimeter sensor ADC readout sample $y[k]$.

In the next sections, two different methods to perform the deconvolution task are presented, in order to recover the sequence $a[k]$, focusing on online reconstruction.

3 Online deconvolution based on FIR filters

Knowing $h[k]$ in advance, it is possible to design a free-running digital filter to compensate for the channel effect and to obtain an online approximation of the target signal $\hat{a}[k]$, as in figure 4a. In most

2019 JINST 14 P12017

of the free-running inverse filter implementations, a delay (Δ) between the digitized samples $a[k]$ and the recovered information is required (typically, Δ is equivalent to the $h[k]$ impulse response length). According to the model presented in figure 3, the experiment specific delay τ was removed before constructing the sequence $h[k]$. Therefore, for total delay computation, the value τ must be added on the top of Δ value, where the later represents only the filter propagation delay. This is not an issue in HEP trigger systems, as far as the total latency of the system stays within the available budget. Currently in ATLAS, for instance, the total delay allowed for the first level trigger is of 100 BC's, which is equivalent to 2.5 µs. However, as will be shown in section 5, typical Δ values for figure 4a are below 21 BCs.

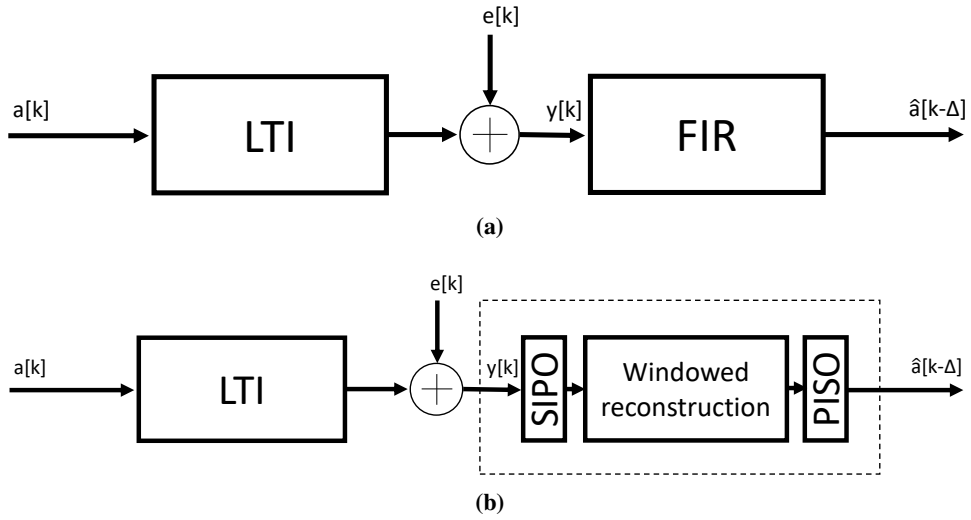

Figure 4. Models to reconstruct the $a[k]$ signal from deconvolution in a free-running environment: (a) FIR filter approach and (b) using a windowed reconstruction (see section 4), which requires two additional systems, Serial Input to Parallel Output (SIPO) and Parallel Input to Serial Output (PISO).

In general, such inverse filter is designed as an Infinite Impulse Response (IIR) Filter [15], since the pole locations are positioned in order to cancel the zeros of $h[k]$ (which is a finite pulse, thus having only zeros) in the Z-transform domain [15]. However, in order to avoid feedback loops in finite-precision numerical implementations, like FPGAs, FIR filter approximations of the IIR filters will be used here. In doing so, the circuitry structure of the reconstruction process becomes similar to the one employed in the standard OF procedures (figure 2). However, some differences may be highlighted:

1. The filter design comes from a totally different paradigm, where the entire pulse information is used instead of restricting to the second-order pile-up statistics.

2. The number of coefficients of the deconvolution filter tends to be higher than the impulse channel response length (M), because it needs tail information from neighbor BC signals in order to promote deconvolution. For standard OF methods, the order is equal to the number of samples of the positive lobule of the reference pulse shape.

3. The peak detector in the FIR filter output is no longer necessary. Instead, a simple threshold must be implemented, removing small negative values due to the electronic noise and residues in the reconstruction process.

2019 JINST 14 P12017

Two deconvolution FIR filter techniques are proposed: the first one applies a deterministic method for obtaining an approximation for the inverse filter based on the LTI impulse response in the Z-transform domain, whereas the second is based on stochastic channel equalization [32], which uses a MSE criterion to minimize the error between the inverse filter output ($\hat{a}[k]$) and the target signal ($a[k]$).

3.1 FIR filter by inverse system approximation

As in [31], $h[k]$ is approximated by the normalized reference pulse shape, since the shaped signal is expected to be invariant to the sampled energy and, thus, is a good approximation for $h[k]$. Small deformations on the reference signal as thermal noise and phase-shifts [45] are not taken into account on the filter design. On the other hand, no Monte Carlo simulation is necessary since only the calorimeter reference pulse shape is used.

Considering the transfer function $F(z)$ as the Z-transform of $h[k]$, an ideal deconvolution (or inverse) filter produces a transfer function $W(z) = 1/F(z)$. The method proposed here consists in obtaining a stable approximate version of $W(z)$ by a FIR filter:

1. Split $W(z)$ into two parts, a stable portion $W_1(z)$ and another unstable $W_2(z)$ (poles outside of the unitary circle), such that $W(z) = W_1(z)W_2(z)$.

2. Invert the convergence region of $W_2(z)$, resulting in a non-causal system $W_2'(z)$, but with a convergence region including the unit circle (a stable non-causal system). The idea behind this approach is to use the stable impulse response $w_2'[k]$ instead of the unstable one $w_2[k]$. This is possible because both responses have the same zero-pole configuration in the Z Transform domain. The drawback is that $w_2'[k]$ is non-causal and requires further treatment for online implementation.

3. As $W_1(z)$ and $W_2'(z)$ are regular IIR filters with exponential decays, their responses must be truncated in order to produce approximate FIR filters $W_1''(z)$ and $W_2''(z)$. The higher the number of used samples more accurate is the impulse response. However, it also increases the final filter order. Thus, truncation must be a compromise between response accuracy and amount of available resources in the FPGA. Since $W_1''(z)$ is causal, its impulse response starts at $k = 0$ and should be truncated to the right. On the other hand, $W_2''(z)$ is non-causal. Then this impulse response finishes at $k = 0$ and must be truncated to the left (negative k samples).

4. $W_2''(z)$ impulse response is non-causal and finite. Thus, applying a proper delay Δ to its discrete-time response shall turn it into a causal system $W_2'''(z)$. Clearly, this delay will propagate to the filter and the final filter response will present a delay (see figure 4), which must be compatible with the trigger system requirements.

5. Using the time-domain impulse responses $w_2'''[k]$ and $w_1''[k]$, which are the inverse Z transforms of $W_2'''(z)$ and $W_1''(z)$, respectively, and performing the convolution between them, the approximate inverse filter impulse response $w[k] = w_2'''[k] * w_1''[k]$ is obtained, where $*$ stands for the discrete convolution operator [15].

2019 JINST 14 P12017

Different from the standard (OF) method filter structure (see figure 2), which has M coefficients, FIR deconvolution filters have a filter order $U > M$ in order to compensate for OOT signals. Usually, a value of U larger than twice the value of M is not necessary for this compensation.

3.2 Inverse filter based on least square error

Alternatively, the channel equalization problem may be solved by finding the vector $\mathbf{w}$ such that, when it is linearly combined with the U latest consecutive samples of $y[k]$ (represented by $\mathbf{y}$), it reconstructs the Minimal Mean Square Error (MMSE) approximation $\hat{a}_j$ for the amplitude of the signal whose peak is located at the j-th tap of the filter:

$$\hat{a}_j = \mathbf{w}^T \mathbf{y}. \tag{3.1}$$

Thus, the cost function is:

$$\Lambda(\mathbf{w}) = E\{(a_j - \mathbf{w}^T \mathbf{y})^2\}, \tag{3.2}$$

where $E\{\cdot\}$ is the expectation operator. Minimizing $\Lambda(\mathbf{w})$ with respect to $\mathbf{w}$ leads to:

$$\frac{d\Lambda(\mathbf{w})}{d\mathbf{w}} = 2E\{\mathbf{y}(a_j - \mathbf{w}^T \mathbf{y})\} = 0, \tag{3.3}$$

which can be rewritten as:

$$\mathbf{w} = \mathbf{R}^{-1}\mathbf{p} \tag{3.4}$$

where $\mathbf{R}$ is the autocorrelation matrix of $\mathbf{y}$ and $\mathbf{p}$ is a vector containing the cross correlation between true value a_j and each component of $\mathbf{y}$. This is known as the Wiener filter [32] and $\mathbf{R}$ and $\mathbf{p}$ may be estimated from a set of a priori known N input-output pairs. Given the $N \times U$ matrix $\mathbf{Y}$ representing a set of N recorded tap vectors $\mathbf{y}$ and $\mathbf{a}$ the $N \times 1$ vector containing the respective true amplitudes, an unbiased estimator for $\mathbf{R}$ is [36]:

$$\hat{\mathbf{R}} = \frac{\mathbf{Y}^T\mathbf{Y}}{N}. \tag{3.5}$$

Similarly, for $\mathbf{p}$:

$$\hat{\mathbf{p}} = \frac{\mathbf{Y}^T\mathbf{a}}{N}. \tag{3.6}$$

Replacing equations. (3.5) and (3.6) in equation (3.4):

$$\hat{\mathbf{w}} = (\mathbf{Y}^T\mathbf{Y})^{-1}\mathbf{Y}^T\mathbf{a}. \tag{3.7}$$

This leads to the LS filter design equation [36]. Different from the Wiener filter, LS does not use the exact value for the second-order statistics $\mathbf{R}$ and $\mathbf{p}$, as presented in equation (3.4). However, providing that a large number of ($\mathbf{y}$, a_j) pairs are known a priori (large N value), this information may be estimated with good accuracy.

When building the ($\mathbf{y}$, a_j) pairs from simulation, the tap index j must be chosen for a specific signal position within the window $\mathbf{y}$. The best choice is to set a_j to the amplitude of the signal whose peak is in the middle of the window, in such a way that all samples of the signal fit within the window (for symmetrical pulses), maximizing amplitude estimation information. In this way, the filter delay response will be half of the window length ($\Delta = U/2$).

2019 JINST 14 P12017

Equation (3.7) was derived considering a zero-mean noise and thus, when this is not true, the noise mean value may propagate through the FIR filter weights producing a bias that deviates the solution from optimal. Since there is no guarantee that the pile-up noise is zero mean (usually it is not), equation (3.7) can be modified for removing any bias:

$$\begin{aligned} \mathbf{Y_2} &= [\mathbf{Y} \quad \mathbf{1}], \\ \hat{\mathbf{w}}_2 &= (\mathbf{Y_2}^T \mathbf{Y_2})^{-1} \mathbf{Y_2}^T \mathbf{a}, \end{aligned} \tag{3.8}$$

where $\mathbf{1}$ is the one vector, which is concatenated to the last column of $\mathbf{Y}$. Thus, the last component of $\hat{\mathbf{w}}_2$ contains the bias value and the other components correspond to the FIR weights. If accurate simulation data are available, this model may handle different noise sources (phase-shift, pulse deformation, cross-talk effects, electronic noise etc.) and high luminosity effects.

4 Windowed iterative techniques for deconvolution

For the windowed methods, instead of using a Shift Register structure like in figure 2, where the $\mathbf{y}$ vector changes for each clock (the filter taps), the algorithm runs over a constant $\mathbf{y}$ vector, previously buffered, reconstructing all the BCs within the buffer simultaneously. Assuming that this process finishes before a new window (with fresh ADC samples) is acquired and some extra circuitries are implemented for data serialization and de-serialization [35], the windowed deconvolution method can be adapted for free-running operation. In this section, a windowed method that uses only addition and multiplication operations is presented, which is feasible for FPGA implementation.

Figure 4b shows the pipeline data-flow structure. An input Serial-to-Parallel (Serial Input to Parallel Output — SIPO) circuitry buffers the next window while the current window is processed by the core circuitry. At the same time, the window computed previously is serialized by the Parallel-to-Serial (Parallel Input to Serial Output — PISO) circuitry. With this architecture, data are delivered in sequence, in an uninterrupted data-flow as requested by a free-running environment. In this approach the delay Δ is fixed as two times the window size ($\Delta = 2U$), regarding SIPO and core circuitries operation time.

For an acquired $\mathbf{y}$ vector of size U and disregarding the electronic noise, the convolution equation may be expressed as a matrix multiplication [32]:

$$\mathbf{y} = \mathbf{H}\mathbf{a}, \tag{4.1}$$

where $\mathbf{H}$ is a $U \times (U - M + 1)$ matrix. This matrix is assembled in such way that each column is a shifted version of $h[k]$. This is a windowed version of the convolution (equation 2.3) for a finite sequence $\mathbf{y}$. If the goal is to reconstruct the vector $\mathbf{a}$ containing the true energy to be estimated, this can be done using the following cost function:

$$Q(\hat{\mathbf{a}}) = |\mathbf{y} - \mathbf{H}\hat{\mathbf{a}}|^2. \tag{4.2}$$

Thus, all components a_j within the window are estimated simultaneously.

2019 JINST 14 P12017

4.1 Gradient Descent (GD) algorithm

A standard iterative approach for minimizing equation (4.2) consists in updating the values of $\hat{\mathbf{a}}$ in the opposite direction of the gradient $\nabla Q = 2\mathbf{H}^T(\mathbf{y} - \mathbf{H}\hat{\mathbf{a}})$, which is known as Gradient Descent (GD) optimization [32]. The iterative process is implemented as follows:

$$\hat{\mathbf{a}}^{i+1} = \hat{\mathbf{a}}^i + \mu\mathbf{H}^T(\mathbf{y} - \mathbf{H}\hat{\mathbf{a}}^i), \tag{4.3}$$

where μ is the step-size on direction to the minimal and i is the iteration index.

It is easy to show that GD algorithm performance is similar to the one of LS FIR filter, since the cost functions in equations (3.2) and (4.2) converge to the same value: both expressions minimize a square value of the error between the parameters and the linear model (written in a different way) [32]. Therefore, there is no advantage of using this approach since the FIR filter reaches the same performance with a lower computational cost. Next, a technique that updates the output $\mathbf{a}$ before each iteration is proposed in order to prioritize non-negative outcomes.

4.2 Positive Gradient Descent (PGD)

The Positive GD (PGD) algorithm operates similarly to the GD, but values of $\hat{\mathbf{a}}^i$ below a certain positive threshold are replaced by zeros at each iteration. This produces a sparse $\hat{\mathbf{a}}$ vector with non-negative components. In this application, the sparse representation [33] tends to concentrate the energy in few positive components, instead of spreading this information erroneously to adjacent collisions, thus reducing the estimation error. A sparse representation for $\mathbf{a}$ in a noisy environment has been shown to be a better approach for deconvolution with respect to simple linear methods [34].

Despite of being an iterative method with a higher computational cost, a free-running execution in modern FPGAs is feasible. The implementation technical details are out of the scope of this paper.

5 Simulation results

A simulation framework was built in order to evaluate the proposed methods for different pile-up levels. A key parameter in this simulation is the occupancy level of the calorimeter cells. As an example, a calorimeter sensor running at 50% of occupancy means that the sensor is hit at every two collisions, on average (which is actually a very harsh situation). The occupancy in a calorimeter sensor depends on several assembly characteristics like the collider luminosity, the calorimeter type (electromagnetic or hadronic), the sensor layer and its pseudorapidity. Therefore, the use of the occupancy as a measurement of the pile-up level avoids the description of all those detector specific parameters. In order to cope with modern calorimetry, the simulation data are generated as follows:

- For a given occupancy, the BC indexes with hits are randomly selected in a set of two million consecutive bunches, half of this sequence being used for the filter design and the other half used for performance studies. The space between bunches is of 25 ns (40 MHz collision rate) as it is in LHC.
- For each selected BC, an energy amplitude value is randomly generated from an exponential distribution, simulating minimum bias events, with mean parameter set to 600 MeV [45–47]. The values coming from this exponential distribution represent the target sequence $a[k]$.

2019 JINST 14 P12017

- Based on the $a[k]$ sequence (target signal), the $y[k]$ sequence (measured signal) is built. This is performed superimposing $h[k]$ sequences (reference pulse-shape) with their amplitudes given by $a[k]$. In this stage, a small pulse phase-shift is chosen from an uniform distribution spanning in ±5 ns before the pulse digitization, representing a small deformation to each pulse.

- Finally, white Gaussian noise is added, with $\sigma = 20$ MeV (typical value in modern calorimetry [48–51]), representing the combination of both readout channel and ADC electronic noises.

Two pulse types were tested: unipolar and bipolar (see figure 5). For sake of reality, those pulse shapes are similar to ATLAS hadronic [17] and electromagnetic [52] calorimeters, respectively, since this is one of the LHC experiments that suffers from intense pile-up effect.

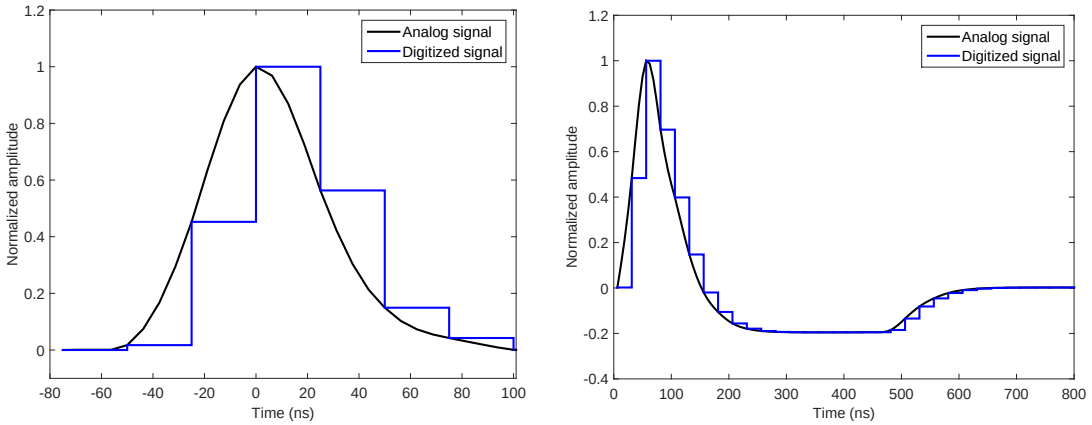

Figure 5. Normalized calorimeter shaped pulses for (a) unipolar and (b) bipolar readout chain simulations.

5.1 FIR design evaluations

The FIR filter order is to be determined, which depends upon the pulse shape and the occupancy level. For this analysis, the LS method was used as the baseline design. Similar results are found for the deterministic FIR filter design as well. Figure 6 shows, for both pulse types, the energy estimation error when different channel occupancy levels and filter order are considered. The performance is computed using the root mean square (RMS) of the error between the estimated ($\hat{a}[k]$) and the truth target amplitude value ($a[k]$), after alignment. For low occupancy, varying the filter order does not bring any improvement. When the occupancy increases, one needs to increase the filter order to keep the error low enough. For the unipolar pulse, the error stabilizes in a minimum value starting from a filter order of 15. Thus, this larger filter order will be used for further analysis. For the bipolar pulse, although the performance keeps improving with the filter order, the gain in performance is not so expressive to justify the use of an order higher than 40. The chosen filter order values 15 and 40 are meant to be satisfactory for the full occupancy range but lower values could be used for low occupancy levels.

2019 JINST 14 P12017

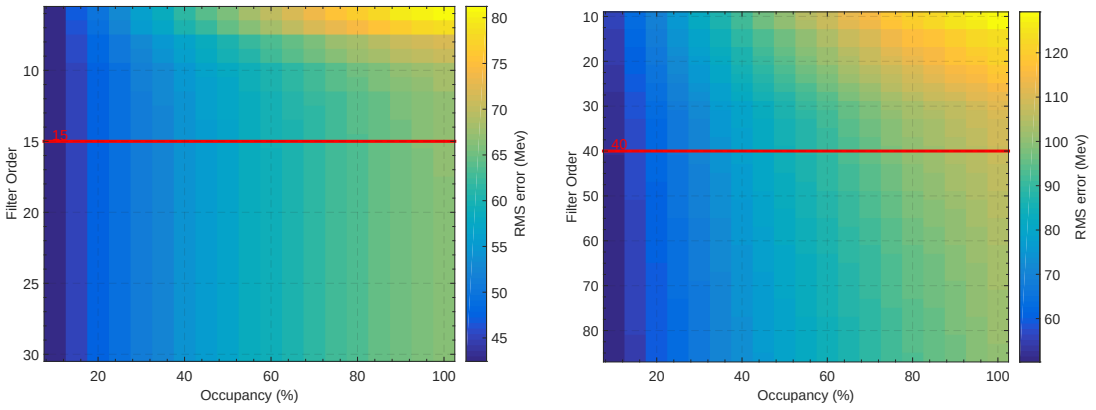

Figure 6. Estimation error as a function of both filter order and occupancy level for the FIR filter based on LS: (a) unipolar and (b) bipolar pulse shapes.

The FIR filter weights, from both pulse types, are shown in figure 7. The position of the most relevant coefficient is at the center. When the pulse peak is in this position, the filter output estimates its amplitude. Therefore, the position of the highest coefficient indicates the delay Δ of the filter response, which is half of the filter order, as expected (the Δ value is either 8 or 21 samples, as for the unipolar and bipolar pulses, respectively).

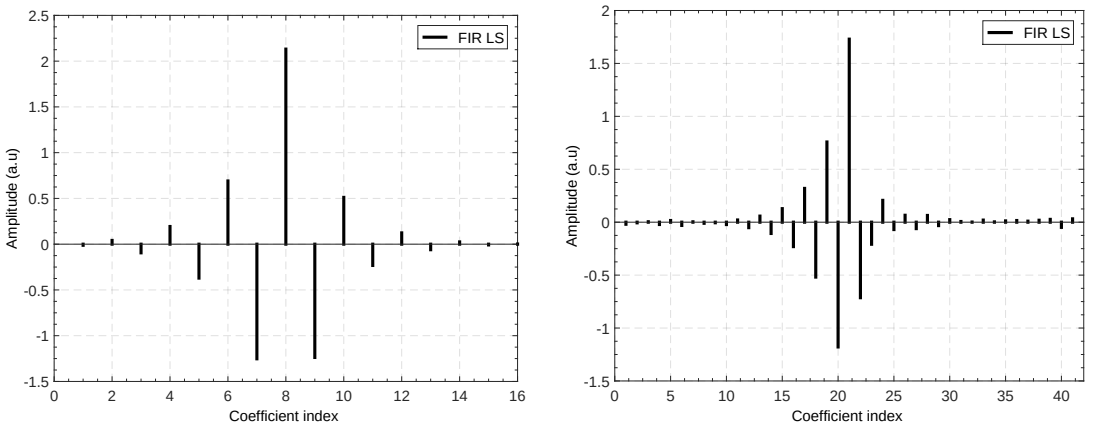

Figure 7. LS FIR filter weights: for (a) unipolar and (b) bipolar pulse-shapes.

A simulation sequence example is shown in the figure 8, which illustrates the energy reconstruction process. The measured sequence ($y[k]$) is also shown. In this example, a channel operating in a 30% occupancy is considered. This occupancy level is very reasonable in some regions of modern calorimeters where pile-up has become an undesirable issue. For sake of comparison, delays concerning calorimeter response and filter process are removed in order to align the signals. On the bottom of each plot, the reconstruction error is shown as well, where one can notice a smaller deviation of the proposed method when compared to OF. Graphically, this discrepancy is more evident for the unipolar pulse.

2019 JINST 14 P12017

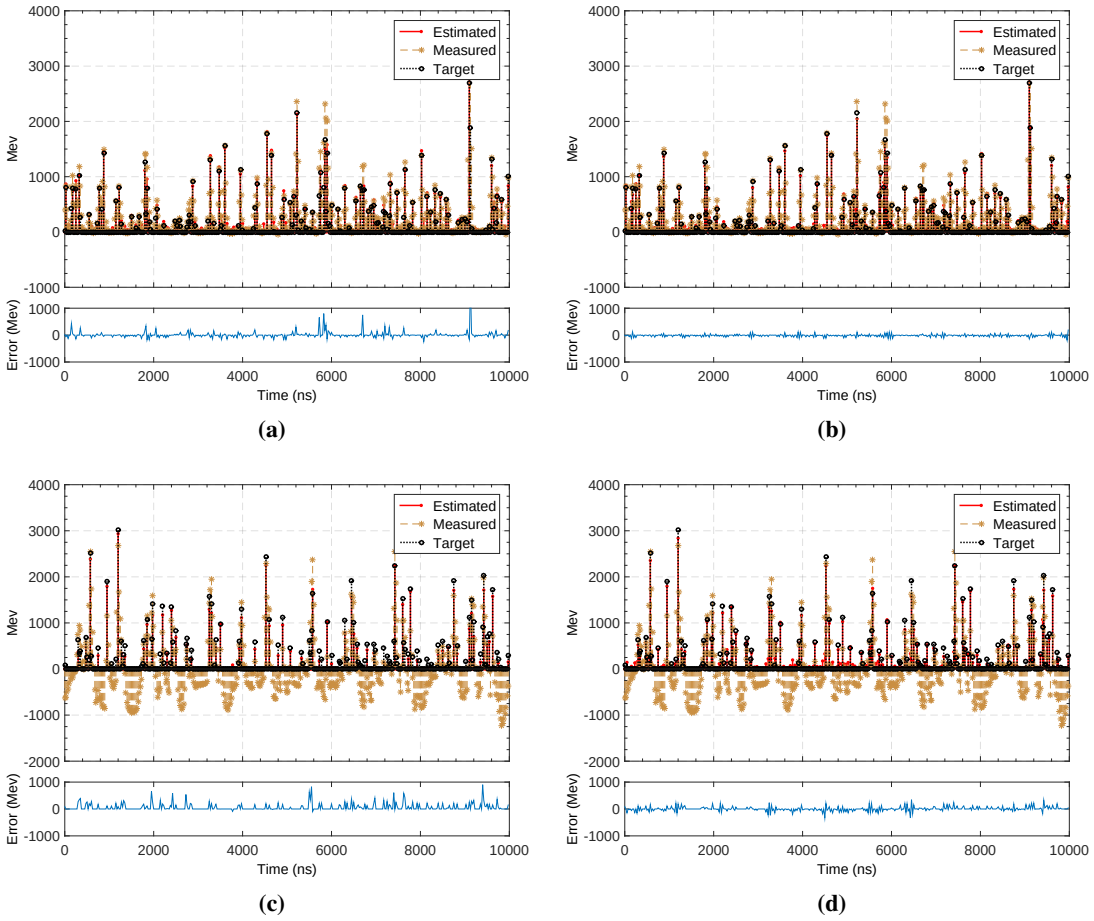

Figure 8. Simulation example for measured, target and estimated signals. The error between estimation and target value is shown on the bottom of each plot. (a) OF and (b) LS filter for unipolar pulse shape, and (c) OF and (d) LS filter for bipolar pulse shape.

5.1.1 FIR filter technique comparisons

This section provides a performance comparison for both deterministic and LS FIR filter designs. Since the deterministic method does not handle noise sources, the main advantage of the LS method is when it operates in low Signal-to-Noise Ratio (SNR) conditions. This statement can be attested from figure 9, which presents the estimation error as a function of the electronic readout noise for both unipolar and bipolar pulses. For the unipolar case, the estimation performance is similar for both design methods when SNR is high (low noise range). For low SNR, the LS method over performs the deterministic one. For the bipolar case, the LS estimation error is lower, even for high SNR. This happens because of the 40-order filter used in this analysis, as the truncation process in the deterministic design still wastes some relevant coefficients. For sake of comparison, the performance for OF is also shown.

It can be concluded from figure 9 that, for high SNR environments, the deterministic approach can be a good choice, since it just requires the pulse-shape information. When SNR is low or the filter order should be as low as possible (for the lack of hardware resources, for instance), the LS method is more indicated. However, it requires an accurate MC simulation.

2019 JINST 14 P12017

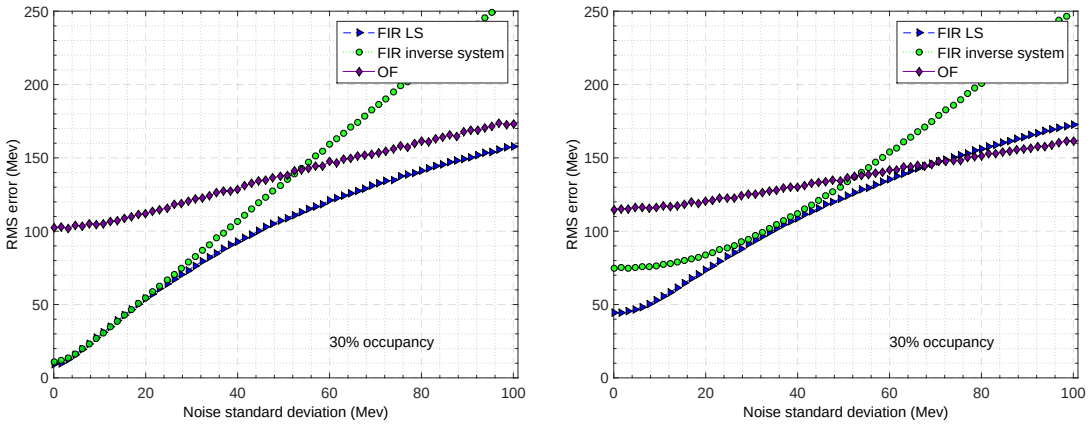

Figure 9. Energy reconstruction error as a function of the Gaussian electronic readout noise for the filter designed techniques considering (a) unipolar and (b) bipolar pulse-shapes.

5.2 Windowed iterative techniques

For the PGD algorithm, it is important to evaluate how the estimation error evolves as the number of iterations increases and the window length varies. As it can be seen from figure 10, for a sensor operating with 30% of occupancy, there is a convergence region where the error stabilizes despite the increase in the window length. From windows lengths larger than 25 samples, for an unipolar pulse shape, and 186 samples for a bipolar one, convergence is achieved. The same behavior is seen for other occupancy levels. Therefore, these window lengths will be kept for further analysis. However, for actual implementation, a compromise between hardware resources and window length should be taken.

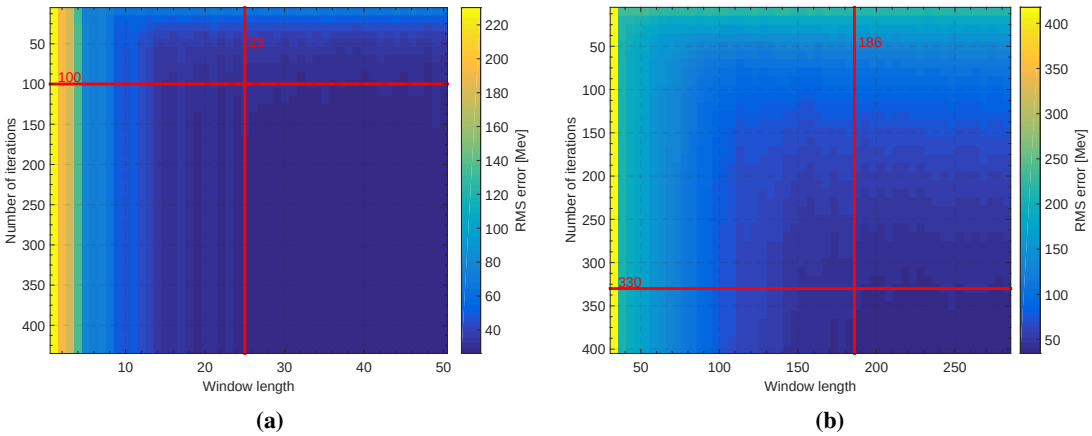

Figure 10. Estimation RMS error due to both window length and number of iterations for the PGD algorithm, considering: (a) unipolar and (b) bipolar pulse shapes.

The required number of iterations may be obtained from fixed window length. Graph slices from figure 10 allow for performance comparison with respect to the number of iterations required

2019 JINST 14 P12017

for convergence, as shown in figure 11. The GD algorithm is also shown as a guideline, since its final error performance is similar to the FIR filter. The PGD algorithm presents smaller final estimation errors. Thus, a performance enhancement is actually achieved when the non-linearity restriction is imposed to each iteration, as in the PGD method. Concerning the feasibility of the implementation, the hardware should be able to run as much iteration as possible during a time interval of U samples (the time used by the SIPO to build the next window). As the iteration process comprises only multiplication and addition operations, a dedicated State Machine [53] can be designed to run in a high-speed fashion in modern FPGAs. To justify the use of this approach, in detrimental of the FIR filter, for the unipolar pulse, for instance, the hardware must be able to implement more than 40 iterations (see figure 11) in the time interval of U samples.

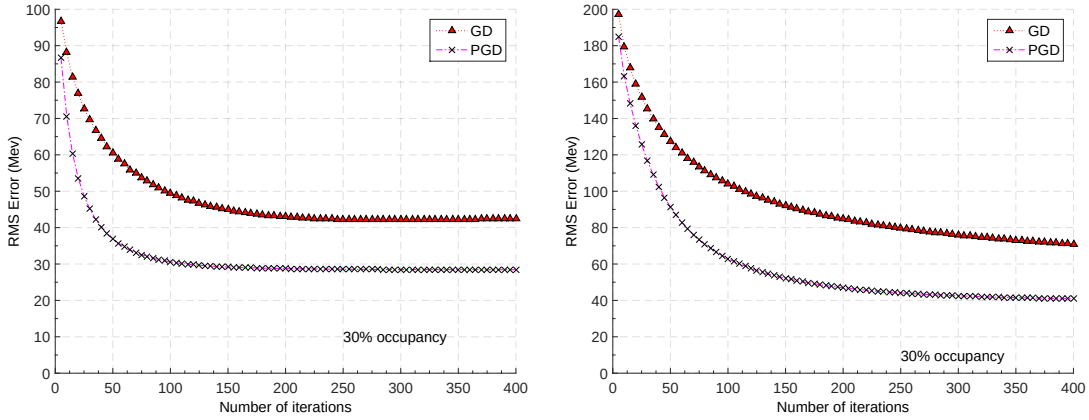

Figure 11. Estimation RMS error as a function of the number of iterations (at 30% occupancy level), considering a window length of 25 and 186 samples, respectively for: (a) unipolar and (b) bipolar pulse shapes.

To conclude the windowed design, it is worth mentioning that, due to the windowing process, reconstruction of the BCs closer to the window edge present higher errors since the signals on the edges are split among adjacent windows. This issue can be solved discarding the edge reconstructions and sliding the window in a step smaller then the window length to make sure that all the BCs will be well reconstructed. For the unipolar pulse, 6 BCs may be discarded on the edges and, thus, the step size becomes 25 – 6 = 19 BCs. For the bipolar pulse, 32 BCs may be discarded, resulting in a step size of 186 – 32 = 154 BCs.

5.3 Online resources

From the aforementioned results, some considerations about resource utilization and response delay can now be outlined. Concerning required hardware resources, the order of the FIR filter based on deconvolution methods tends to be higher than the ones from standard methods. For the unipolar pulse case, the filter order values for standard OF and deconvolution methods are 6^{th} [17] and 15^{th} respectively. For the bipolar pulse, standard methods use only the positive lobule, which comprises only 5 samples [40, 47]. On the other hand, deconvolution FIR filter requires a much higher order for this kind of pulse due to its long negative tail. In the filter designed here, a high

2019 JINST 14 P12017

filter order was used, to cope with very high occupancies. However, modern FPGA architectures are able to implements high-order FIR filters with high speed, in such a way that the filter order is not a remarkable constraint. Besides, the filter order, for deconvolution, can be better calibrated depending on the occupancy level (see figure 6).

The resources for the windowed methods are more difficult to dimension and compare, since it will depend on the design architecture. Actually, if a sequential design, in a high speed embedded processor or state machine, is employed, the hardware resources can be comparable (or even lower) than a direct FIR filter implementation. In the case of a parallel implementation, the amount of hardware resources can be higher, but the electronic speed-grade decreases. Since the circuitry is based on matrix operations, one important parameter to pay attention here is the window size U — the hardware complexity (or processing speed) will increase with U^2.

Other important constraint, mainly in trigger system implementation, is the delay response Δ. In the FIR filter designed here, the delay was calibrated to match half of the filter order ($\Delta = U/2$). Therefore, the delay for the unipolar and bipolar pulses are 8 and 20 BCs, respectively, against 6 and 4 BCs for the standard OF implementation (the pulse peak position plus 2 BCs for the peak detector [16]). However, for both deconvolution FIR filter designs proposed here, the delay can be calibrated to match the trigger system requirement regardless the filter order. The compromise between the allowed delay and the reconstruction performance is application dependent.

Different from the FIR filter design, the Δ delay for the windowed methods must be fixed on twice the window size ($\Delta = 2U$). This is due to the pipeline architecture necessary to adapt the windowed operation to a free-running environment. Therefore, this method should be used in systems that allow a higher delay response. For the filters designed here, the delays are 50 and 372 BCs, considering the unipolar and the bipolar pulses, respectively.

5.4 Reconstruction performance

The energy estimation error as a function of the occupancy level is shown in figure 12 for all methods. It is worth mentioning that the OF design is properly evaluated here, as the pile-up information is taken into account in its noise covariance matrix ($\mathbf{C}_\epsilon$) by applying equation (2.2). Despite the pulse shape type, it can be observed that in a low pile-up scenario (occupancy ≈ 0) the OF is a quite good estimation method, as expected. However, as the pile-up level increases (high occupancy levels and the pulse shape deviates from the expected fixed shape) OF method fails to reconstruct the correct energy values. The FIR based on methods presented relatively low estimation errors and represent a reasonable choice due to their simpler implementations. For the highest performance, PGD is the best option for realistic occupancy levels (up to 60%). As the occupancy increases, the iterative method starts failing, since the number of superimposed signals is too high to accomplish a sparse representation and the LS FIR filter becomes the best option.

The main reason for the low performance of the OF method is the interpretation of signal pile-up as a noise source and its restricted statistical information usage, as only second-order statistics is considered in its design. Besides, the peak detector only performs a correct reconstruction when there are empty bunches around the central one (low occupancy). On the other hand, the deconvolution methods interpret the pile-up as actual signals and remove the necessity of a peak detector, performing good reconstruction even for very high pile-up levels.

2019 JINST 14 P12017

For the reference SNR used here (20 MeV electronic noise), both the deterministic and LS FIR filter designs exhibit similar performance, for the unipolar case, because the SNR is considerably high. For the bipolar pulse, LS FIR filter presents better performance, indicating that a filter order higher than 40 may increase performance. However, higher-order filters require more hardware resources and produce larger delays.

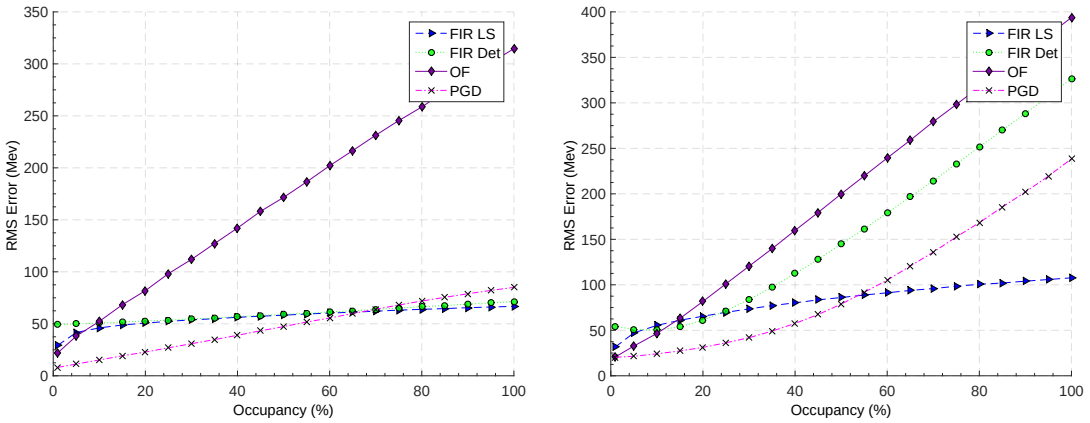

Figure 12. Energy reconstruction performance as a function of occupancy levels: (a) unipolar and (b) bipolar pulse-shapes.

The table 1 summarizes results and shows the RMS error for 30% occupancy. The error for OF is higher than the one produced by any proposed method, being 100% higher for the unipolar pulse when comparing with the worst deconvolution approach (the FIR inverse system). Next to this method, the FIR LS presents a small increasing in the performance, due to the additive noise and the pulse shape deformation (phase shift). As the FIR inverse system, the PDG uses only the pulse shape information. However, the later presents the best performance due to its connection with SR, which is known as a good denoising technique.

Table 1. Result summary for the unipolar and bipolar pulse shape considering 30 % occupancy.

Algorithm	RMS error (Mev) for unipolar	RMS error (Mev) for bipolar
OF	112	120
FIR inverse system	55	84
FIR LS	54	74
PGD	31	42

6 Conclusions

This paper proposed and evaluated, through simulation data, online deconvolution methods that may be applied to high-energy calorimeters operating at high-event rates (intense pile-up scenario). Two classes of algorithms were proposed, one based on FIR inverse filters and another based on iterative GD algorithms. By comparing the proposed methods for typical unipolar and bipolar

shaped calorimeter pulses and different pile-up levels (occupancies), it was observed that the best energy estimation results were obtained for the iterative method when higher pile-up levels are of concern. However, FIR filters may not be discarded, as they are quite simple to implement. The iterative algorithm uses only adders and multiplies (feasible for FPGA implementation) and it is able to process several BCs in parallel, which is very attractive even for higher trigger levels.

Acknowledgments

The authors would like to thank CNPq, CAPES, RENAFAE, FAPERJ, FAPEMIG, FAPESB (Brazil) and CERN (Switzerland) for their support to this work.

References

[1] O. Bruning and L. Rossi, *The High Luminosity Large Hadron Collider. The New Machine for Illuminating the Mysteries of Universe*, Advanced Series on Directions in High Energy Physics, volume 24, World Scientific (2015).

[2] S. Ozaki and T. Roser, *Relativistic heavy ion collider, its construction and upgrade*, *Prog. Theor. Exp. Phys.* **2015** (2015) 3A102.

[3] Pierre Auger collaboration, *The Pierre Auger Cosmic Ray Observatory*, *Nucl. Instrum. Meth.* **A 798** (2015) 172 [arXiv:1502.01323].

[4] FCC collaboration, *FCC-ee: The Lepton Collider*, *Eur. Phys. J. Spec. Top.* **228** (2019) 261.

[5] W. Barletta et al., *Future hadron colliders: From physics perspectives to technology R&D*, *Nucl. Instrum. Meth.* **A 764** (2014) 352.

[6] R. Wigmans, *Calorimetry: Energy Measurement in Particle Physics*, second edition, Oxford University Press, Oxford U.K. (2018).

[7] ATLAS collaboration, *The Run-2 ATLAS Trigger System*, *J. Phys. Conf. Ser.* **762** (2016) 012003.

[8] CMS collaboration, *The CMS trigger system*, 2017 *JINST* **12** P01020 [arXiv:1609.02366].

[9] T.N. Takahashi et al., *The electronics, online trigger system and data acquisition system of the J-PARC E16 experiment*, *J. Phys. Conf. Ser.* **664** (2015) 082053.

[10] ATLAS collaboration, *Technical Design Report for the Phase-II Upgrade of the ATLAS TDAQ System*, CERN-LHCC-2017-020 (2017) [ATLAS-TDR-029].

[11] Y. Nakahama, *The ATLAS Trigger System: Ready for Run-2*, *J. Phys. Conf. Ser.* **664** (2015) 082037.

[12] ALICE collaboration, *Real-time data processing in the ALICE High Level Trigger at the LHC*, *Comput. Phys. Commun.* **242** (2019) 25 [arXiv:1812.08036].

[13] K. Anderson et al., *Front-end Electronics for the ATLAS Tile Calorimeter*, in proceedings of the *4th Workshop on Electronics for LHC Experiments (LEB 98)*, Rome, Italy, 21–25 September 1998.

[14] B. Åsman et al., *The ATLAS Level-1 Calorimeter Trigger: PreProceSSOR implementation and performance*, 2012 *JINST* **7** P12008.

[15] S.K. Mitra and Y. Kuo, *Digital signal processing: a computer-based approach. Volume 2*, McGraw-Hill, New York U.S.A. (2006).

[16] J. Bystricky et al., *Algorithms and architecture for the L1 calorimeter trigger at D0 Run IIB*, *IEEE Trans. Nucl. Sci.* **51** (2004) 351.

2019 JINST 14 P12017

[17] B.S. Peralva, *The TileCal energy reconstruction for collision data using the matched filter*, in proceedings of the *IEEE Nuclear Science Symposium and Medical Imaging Conference (2013 NSS/MIC)*, Seoul, South Korea, 27 October–2 November 2013, pp. 1–6.

[18] The CMS Electromagnetic Calorimeter Group, *Reconstruction of the signal amplitude of the CMS electromagnetic calorimeter*, *Eur. Phys. J.* **C 46S1** (2006) 23.

[19] E. Fullana et al., *Digital signal reconstruction in the ATLAS hadronic tile calorimeter*, in proceedings of the *14th IEEE-NPSS Real Time Conference*, Stockholm, Sweden, 4–10 June 2005, p. 4.

[20] G. Bertuccio, E. Gatti, M. Sampietro, P. Rehak and S. Rescia, *Sampling and optimum data processing of detector signals*, *Nucl. Instrum. Meth.* **A 322** (1992) 271.

[21] V. Polushkin, *Nuclear Electronics: Superconducting Detectors and Processing Techniques*, Wiley (2004).

[22] G. Apollinari, O. Brüning, T. Nakamoto and L. Rossi, *High Luminosity Large Hadron Collider HL-LHC*, *CERN Yellow Rep.* (2015) 1 [arXiv:1705.08830].

[23] ATLAS collaboration, *Simulation of Pile-up in the ATLAS Experiment*, *J. Phys. Conf. Ser.* **513** (2014) 022024.

[24] L. Evans and P. Bryant, *LHC Machine*, 2008 *JINST* **3** S08001.

[25] ATLAS collaboration, *The ATLAS Experiment at the CERN Large Hadron Collider*, 2008 *JINST* **3** S08003.

[26] CMS collaboration, *The CMS Experiment at the CERN LHC*, 2008 *JINST* **3** S08004.

[27] W.E. Cleland and E.G. Stern, *Signal processing considerations for liquid ionization calorimeters in a high rate environment*, *Nucl. Instrum. Meth.* **A 338** (1994) 467.

[28] ATLAS collaboration, *Technical Design Report for the Phase-II Upgrade of the ATLAS LAr Calorimeter*, CERN-LHCC-2017-018 (2017) [ATLAS-TDR-027].

[29] ATLAS collaboration, *Technical Design Report for the Phase-II Upgrade of the ATLAS Tile Calorimeter*, CERN-LHCC-2017-019 (2017) [ATLAS-TDR-028].

[30] CMS HCAL collaboration, *New method of out-of-time energy subtraction for the CMS hadronic calorimeter*, *J. Phys. Conf. Ser.* **1162** (2019) 012036.

[31] L.M. de Andrade Filho, B.S. Peralva, J.M. de Seixas and A.S. Cerqueira, *Calorimeter Response Deconvolution for Energy Estimation in High-Luminosity Conditions*, *IEEE Trans. Nucl. Sci.* **62** (2015) 3265.

[32] S. Haykin, *Adaptive Filter Theory*, fifth edition, Pearson (2014).

[33] M. Elad, *Sparse and redundant representation*, Springer (2010).

[34] D.P. Barbosa, L.M. de Andrade Filho, B.S. Peralva, A.S. Cerqueira and J.M. de Seixas, *Sparse representation for signal reconstruction in calorimeters operating in high luminosity*, *IEEE Trans. Nucl. Sci.* **64** (2017) 1942.

[35] U. Meyer-Baese, *Digital Signal Processing with Field Programmable Gate Arrays (Signals and Communication Technology)*, Springer-Verlag (2004).

[36] S.M. Kay, *Fundamentals of statistical signal processing. Volume I: Estimation theory*, first edition, Pearson (1993).

[37] CMS collaboration, *CMS electromagnetic trigger commissioning and first operation experiences*, *J. Phys. Conf. Ser.* **160** (2009) 012062.

2019 JINST 14 P12017

[38] Y. Sugiyama et al., *The Data Acquisition System for the KOTO Experiment*, *IEEE Trans. Nucl. Sci.* **62** (2015) 1115 [arXiv:1406.3907].

[39] J. Keil, *Operational experience with HERA*, in proceedings of the *2007 IEEE Particle Accelerator Conference (PAC)*, Albuquerque, NM, U.S.A., 25–29 June 2007, pp. 1932–1934.

[40] V. Radeka, *Low-noise techniques in detectors*, *Annu. Rev. Nucl. Part. Sci.* **38** (1988) 217.

[41] H.L. Van Trees, *Detection, estimation, and modulation theory. Part I: Detection, estimation, and linear modulation theory*, John Wiley & Sons (2004).

[42] R.B. Millar, *Maximum likelihood estimation and inference: with examples in R, SAS and ADMB. Volume 11*, John Wiley & Sons (2011).

[43] H.V. Poor, *An introduction to signal detection and estimation*, Springer Science & Business Media (2013).

[44] E. Fullana et al., *Optimal Filtering in the ATLAS Hadronic Tile Calorimeter*, ATL-TILECAL-2005-001 (2005).

[45] J. Chapman, *ATLAS simulation computing performance and pile-up simulation in ATLAS*, in proceedings of the *1st LPCC Detector Simulation Workshop*, CERN, Meyrin, Switzerland, 6–7 October 2011.

[46] S. Banerjee, *CMS simulation software*, *J. Phys. Conf. Ser.* **396** (2012) 022003.

[47] M. Aleksa et al., *ATLAS Liquid Argon Calorimeter Phase-I Upgrade Technical Design Report*, CERN-LHCC-2013-017 (2013) [ATLAS-TDR-022].

[48] ATLAS LAr collaboration, *Electronic calibration of the ATLAS LAr calorimeter and commissioning with cosmic muon signals*, *J. Phys. Conf. Ser.* **160** (2009) 012050.

[49] G. Drake, D. Frei, S.R. Hahn, C.A. Nelson, S.A. Segler and W. Steurmer, *The Upgraded CDF front end electronics for calorimetry*, *IEEE Trans. Nucl. Sci.* **39** (1992) 1281.

[50] U. Behrens et al., *Calibration of the forward and rear ZEUS calorimeter using cosmic ray muons*, *Nucl. Instrum. Meth.* **A 339** (1994) 498.

[51] ATLAS Liquid Argon Calorimeter Group, *AREUS: A Software Framework for ATLAS Readout Electronics Upgrade Simulation*, *EPJ Web Conf.* **214** (2019) 02006.

[52] S.A. Majewski, *Electronic readout of the ATLAS liquid argon calorimeter: Calibration and performance*, in proceedings of the *2010 17th IEEE-NPSS Real Time Conference*, Lisbon, Portugal, 24–28 May 2010, pp. 1–5.

[53] R. Tocci, N. Widmer and G. Moss, *Digital Systems*, twelveth edition, Pearson (2016).

2019 JINST 14 P12017